ELSEVIER

Nuclear Instruments and Methods in Physics Research A 421 (1999) 322–333

NUCLEAR INSTRUMENTS & METHODS IN PHYSICS RESEARCH Section A

A CMOS detector leakage current self-adaptable continuous reset system: Theoretical analysis

Gianluigi De Geronimo*, Paul O'Connor

Brookhaven National Laboratory, Instrumentation Division, Bldg. 535B, Upton, NY 11973, USA

Received 2 June 1998; received in revised form 11 August 1998

Abstract

A continuous reset system for the discharge of the feedback capacitance of integrated charge preamplifiers is presented. The system, based on the use of a FET operating in the saturation region, is self-adaptable with respect to a wide range of detector leakage currents. A circuit which provides compensation of the signal from the charge amplifier is also proposed. The noise analysis, which takes into account both the stationary and non-stationary noise contributions and the effect of the rate, shows that the system, when carefully designed, can offer good signal/noise performance for applications in γ-ray and high-energy X-ray spectroscopy. Practical layout considerations are also made. © 1999 Elsevier Science B.V. All rights reserved.

PACS: 29

Keywords: Reset system; CMOS

1. Introduction

In an ionizing radiation detection system, the charge released by a radiation detector after each ionizing event is usually collected by a charge amplifier, which provides the signal integration and the first amplification through the feedback capacitance. When a series of charge pulses is released by the detector, the total charge accumulated by the feedback capacitance may lead to the amplifier saturation. Target of a reset system is the discharge of the feedback capacitance in order to avoid the amplifier saturation, without degrading the noise and linearity performances of the overall system. In the ever more frequent case of a large number of detection channels *dc-coupled* to the integrated front-end electronics, the reset system should also supply the detector leakage current, which is subject to wide changes due to thermal effects, degradation and spreading in the technology dependent parameters. The classical solution based on the use of a simple resistor in parallel to the feedback capacitance becomes in most cases impracticable. As a consequence, continuous and switched integrated reset systems based on active devices have been proposed [1–12].

* Corresponding author. Tel.: + 1 516 344 5336; fax: + 1 516 344 5773; e-mail: degeronimo@bnl.gov.

0168-9002/99/$ – see front matter © 1999 Elsevier Science B.V. All rights reserved.
PII: S0168-9002(98)01218-2

Aim of this work is the theoretical analysis of a simple continuous reset system, based on the use of a single p-channel MOSFET operating in the saturation region. The analysis is carried out in view of an integrated front-end electronics for γ-ray and high-energy X-ray spectroscopy with CZT pixel detectors, characterized by a leakage current in the nA range, but it can be easily extended to other cases and applications.

2. The reset circuit

2.1. Static analysis

A schematic of the proposed reset system is shown in Fig. 1. M_1 is a p-channel MOSFET that is assumed to operate in the saturation region, and this is the main difference with respect to a previously proposed system [6,7]. To this aim the gate bias voltage V_{GG} must be chosen in order to satisfy the condition $|V_{DG1}| > |V_{T1}|$ where V_{T1} is the threshold voltage of M_1. In this first analysis the quadratic approximation $I_{D1} = k'/2(W_1/L_1)(V_{GS1} - V_{T1})^2$ for the drain current of M_1 will be used.

If I_{DET} is absent or negligible, the drain current I_{D1} of M_1 equals the input bias current I_B of the voltage amplifier A_1. The gate bias voltage V_{GG} and the drain current I_{D1} set the dc level of the output voltage V_{OUT}, which is higher than the dc level of the input voltage V_{IN} in order to satisfy the condition $|V_{DS1}| > |V_{GS1} - V_{T1}|$. As an increase of V_{OUT} at a constant I_{D1} $(= I_B)$ would increase V_{IN} depending on the transconductance of M_1 and on the differential resistance of the input node, the stabilization of the bias point of the charge amplifier is achieved.

If I_{DET} increases or it is not negligible, the drain current I_{D1} of M_1 increases accordingly, as well as the dc level of the output voltage V_{OUT}. It is easy to verify that, under the given assumptions and the further assumption that A_1 is ideal, the dependence of V_{OUT} on I_{DET} can be approximated by

$$V_{OUT} \approx V_{GG} - V_{T1} + \sqrt{\frac{2}{k'}\frac{L_1}{W_1}(I_{DET} + I_B)}, \qquad (1)$$

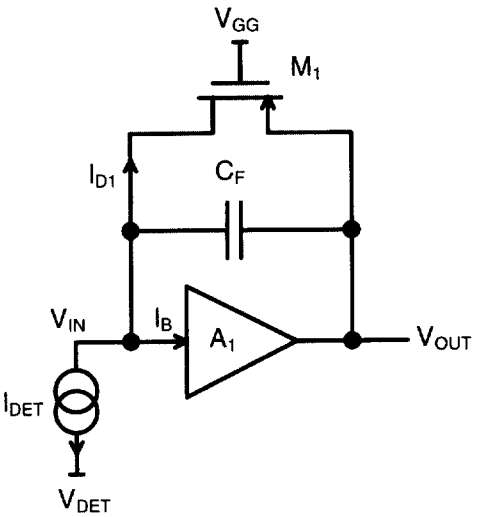

Fig. 1. Schematic of the proposed reset sytem.

where $k' = C_{ox}\mu_p$, and L_1 and W_1 are, respectively, the gate length and width of M_1. In Fig. 2 is shown V_{OUT} versus I_{DET} as predicted by Eq. (4) and by a HSPICE BSIM level 13 simulation. For this example, $k' = 25.8\ \mu A/V^2$, $V_{T1} = -1.37$ V, $L_1 = 60\ \mu m$, $W_1 = 1.8\ \mu m$, and $V_{GG} = -1$ V have been chosen. The difference between the two predictions is due to the limits of the quadratic approximation, which does not consider the body effect and the behavior of M_1 in the moderate and weak inversion regions of operation.

From Fig. 2 it can be observed how the system can supply changes of I_{DET} up to several orders of magnitude with relatively small changes of the charge amplifier dc output voltage V_{OUT}.

2.2. Dynamic analysis

As a response to a $\delta(t)$-like pulse of negative charge Q_{DET} from the detector (see Fig. 3), the feedback capacitance C_F is instantaneously charged by an amount $Q_C = Q_{DET}$, and at the output appears a positive voltage signal which at $t = 0$ is given by $v_{out}(0) = Q(0)/C_F$. The gate to source voltage $|v_{gs1}|$ of M_1 decreases accordingly, and a drain current i_{d1}, which discharges C_F, is generated.

Because of the nonlinear dependence of i_d on v_{gs}, the time dependence of the discharge of the input

node does not show a simply exponential behavior, as in the case of a feedback resistor. By using for simplicity the quadratic approximation, the dependence can be evaluated by using the KCL at the input node:

$$Q_{DET}\delta(t) = C_F \frac{dv_{out}}{dt} + \frac{1}{2} k' \frac{W_1}{L_1} \times [v_{out}^2 - 2v_{out}(V_{GS1} - V_{T1})], \quad (2)$$

where V_{GS} is the dc gate to source voltage. This first order nonlinear differential equation in v_{out}, known as Riccati equation, can be transformed into a linear equation and solved [13] for $t > 0$, giving

$$v_{out}(t) = \frac{2(V_{GS1} - V_{T1})}{\frac{K}{V_{GS1} - V_{T1}} \frac{C_F}{k'} \frac{L_1}{W_1} \exp\left[\frac{-t}{C_F} k' \frac{W_1}{L_1} (V_{GS1} - V_{T1})\right] + 1}, \quad (3)$$

where K is a constant which can be determined by applying the boundary condition $v_{out}(0) = Q_{DET}/C_F$. By considering that $-k'(W_1/L_1)(V_{GS1} - V_{T1})$ is the transconductance g_{m1} of M_1 at the operating point, it finally results in

$$v_{out}(t) = \frac{2(V_{GS1} - V_{T1})}{\left[2(V_{GS1} - V_{T1}) \frac{C_F}{Q_{DET}} - 1\right] \exp\left(\frac{t}{C_F} g_{m1}\right) + 1}. \quad (4)$$

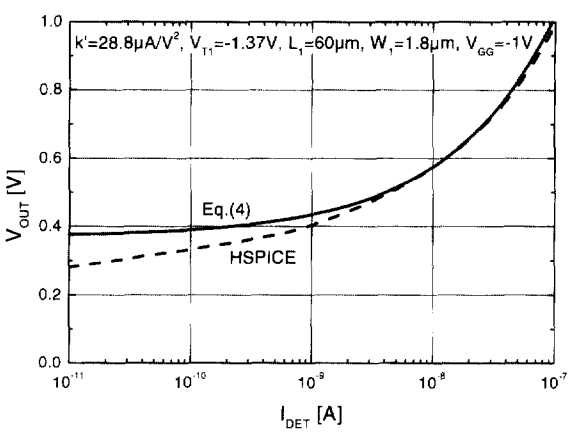

Fig. 2. Theoretical and simulated dependence of V_{OUT} on I_{DET} for the circuit of Fig. 1.

For low enough values of Q_{DET}, such that $v_{out}(0) \ll 2(V_{GS1} - V_{T1})$, $v_{out}(t)$ reduces to a simple exponential function with amplitude proportional to Q_{DET} and decay time constant C_F/g_{m1}. For higher values of Q_{DET}, $v_{out}(t)$ is a non-exponential function, with shape dependent on Q_{DET}. It is worth noting that v_{out} depends on I_{DET} through the term

$$V_{GS1} - V_{T1} = -\sqrt{\frac{2}{k'} \frac{L_1}{W_1} (I_{DET} + I_B)}. \quad (5)$$

In Fig. 4a is shown the function $v_{out}(t)$ as predicted by Eq. (4) and by a HSPICE BSIM level 13 simulation. For this example, $I_{DET} = 1$ nA, $C_F = 100$ fF, $Q_{DET} = 100$ fC and the same values of k', V_{T1}, L_1, W_1, V_{GG} of previous example have been assumed. For comparison, in Fig. 4a is also shown an exponential shape. Fig. 4b shows $v_{out}(t)$, normalized to the peaking value Q_{DET}/C_F, for different values of Q_{DET}.

It is straightforward that a compensation circuit must be used in order to minimize the non-linearity introduced by the dependence of v_{out} on Q_{DET} and the dependence of Q_{DET} on the parameters of the active device M_1.

2.3. Compensation circuit

The schematic of the reset system with the compensation circuit is shown in Fig. 5 and it is similar

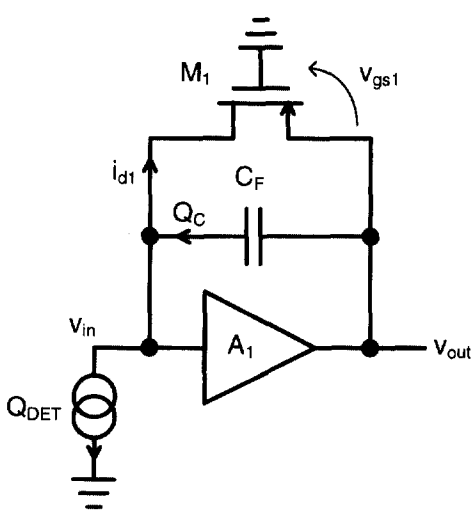

Fig. 3. Schematic of the reset system for the dynamic analysis.

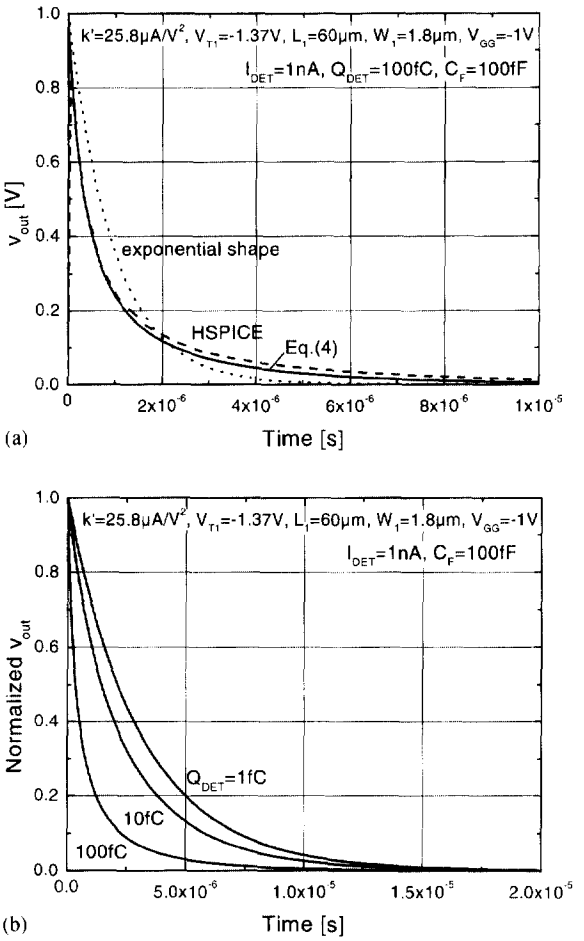

Fig. 4. Time dependence of v_{out} for $I_{DET} = 1$ nA and $C_F = 100$ fF: (a) case $Q_{DET} = 100$ fC, compared to an exponential shape; (b) normalized, for different values of Q_{DET}.

to a previously proposed configuration [6,7]. The compensation is based on the use of a second p-channel transistor M_2 with the source and the gate connected respectively to the source and the gate of M_1. The drain of M_2 must be connected, as shown in Fig. 5, to the input of a transimpedance stage (for instance the first stage of a shaper amplifier), with input dc voltage V_{in2} equal or close to that of A_1.

In order to achieve the compensation, the gate length and width of M_2 must respectively satisfy the conditions $L_2 = L_1$ and $W_2 = N \times W_1$, where

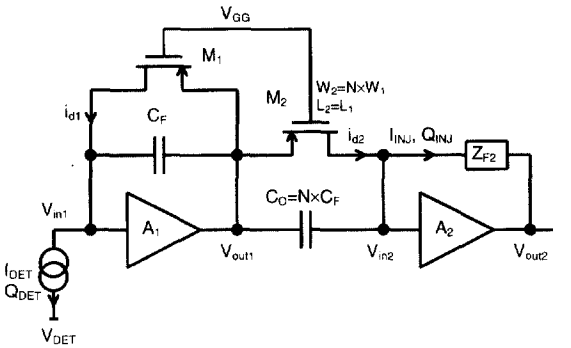

Fig. 5. Schematic of the reset system including the compensation circuit and the first stage of the shaper amplifier (A_2, Z_{F2}).

L_1 and W_1 are the gate length and width of M_1 and N is the ratio C_O/C_F between the coupling capacitance C_O and the feedback capacitance C_F. If these conditions are satisfied, the drain current of M_2 is N times the drain current of M_1.

From a static point of view it results that the dc current I_{INJ} injected in the transimpedance amplifier is N times the detector leakage current I_{DET}, and the output dc level V_{out2} is set accordingly, depending on the value of the dc resistive component of Z_{F2}.

From a dynamic point of view, the charge pulse Q_{INJ} injected in the transimpedance amplifier can be evaluated, and it follows:

$$Q_{INJ} = \int \left[C_O \frac{dv_{out1}(t)}{dt} + i_{d2}(t) \right] dt$$

$$= N \int \left[C_F \frac{dv_{out1}(t)}{dt} + i_{d1}(t) \right] dt = N Q_{DET}, \quad (6)$$

where $i_{d1}(t)$ and $i_{d2}(t)$ are, respectively, the drain currents of M_1 and of M_2 which are due to the reset. Eq. (6) shows that the charge Q_{INJ} injected in the transimpedance amplifier is proportional to the charge Q_{DET} released by the detector. Due to the finite speed of M_1, M_2 and A_1, the width of the injected charge pulse Q_{INJ} is larger than the corresponding width of the charge pulse Q_{DET}, but

the ratio N between the total Q_{INJ} and the total Q_{DET} is preserved.

In Fig. 6a are shown, as results of a HSPICE BSIM level 13 simulation, the time dependence of the total charge Q_{INJ} injected in Z_{F2} and the charge per unit of time dQ_{INJ}/dt, for $I_{DET} = 100$ fC. A -1000 finite gain and a dominant pole with 1 μs time constant have been assumed for the amplifier A_1. From Fig. 6a it can be observed that the compensation is effective and that total charge injected in Z_{F2} reaches the expected value $Q_{INJ} = N \times Q_{DET} = 10$ pC, in this case, in less than 50 ns. In Fig. 6b the time dependence of the total injected charge Q_{INJ} for different values of Q_{DET} is shown. An integral linearity error below 1‰ has been verified from the simulation.

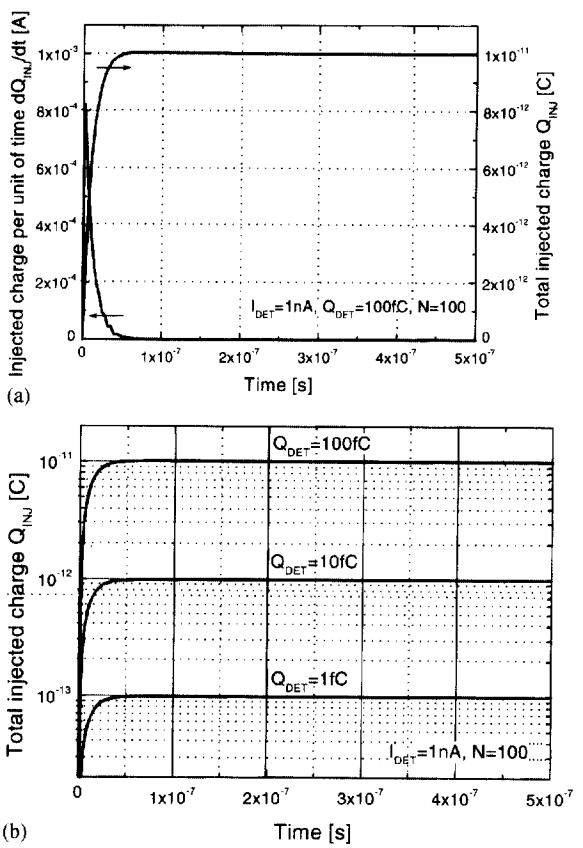

Fig. 6. Total charge Q_{INJ} injected in Z_{F2} versus the time: (a) for $Q_{DET} = 100$ fC, together with the charge per unit of time dQ_{INJ}/dt; (b) for $Q_{DET} = 1$, 10 and 100 fC.

2.4. Noise analysis

The schematic of the reset system for the evaluation of the Equivalent Noise Charge (ENC) is shown in Fig. 7. The noise contributions from the following generators are considered: (i) noise generator i_{nDET} associated to the shot noise of the detector leakage current, with power spectrum qI_{DET}; (ii) noise generator i_{n1} associated to the drain current of M_1, composed of a $1/f$ term with power spectrum $g_{m1}^2 A_{f1}/f$, where $A_{f1} = K_{f1}/(C_{ox}W_1L_1)$ [14,15], plus a white term with power spectrum $\alpha_1\eta_1 2kTg_{m1}$ where α_1 is a coefficient which depends on the level of inversion ($\alpha_1 = 1/2$ in weak inversion and $\alpha_1 = 2/3$ in strong inversion) and η_1 is a coefficient which takes into account the effect of the fixed bulk charges on g_{m1} ($\eta_1 > 1$) [15–19]; (iii) noise generator i_{n2} associated to the drain current of M_2, with the same terms of i_{n1}; (iv) equivalent input voltage noise v_{nA} of A_1 composed of a $1/f$ term with power spectrum A_{fA}/f, plus a white term with power spectrum $\alpha_A\eta_A\gamma_A\, 2\,kT/g_{mA}$ where g_{mA} in the transconductance of the input FET and γ_A takes into account the hot electron effect; and (v) noise generator i_{nF2} associated to the thermal noise of Z_{F2}, given by $2kT\,\mathrm{Re}\{1/Z_{F2}\}$. The equivalent input voltage noise v_{nA2} of A_{12} will be neglected assuming that $v_{nA1}(C_{in}/C_F)^2 \gg v_{nA2}$. In all the cases the power spectrum is considered bilateral with exception of the $1/f$ noise for which the unilateral representation is used.

In the noise evaluation, the *non-stationary* noise contributions related to the reset current i_{d1} must

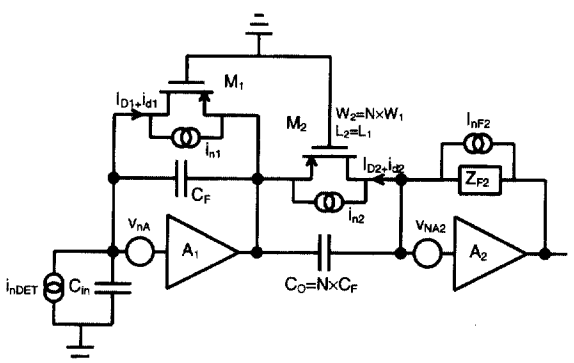

Fig. 7. Schematic of the reset system for the evaluation of the ENC.

also be considered. These additional contributions are due to the fact that, at each charge pulse released by the detector, the corresponding reset current i_{d1} temporarily increases the value of g_{m1} and g_{m2}.

2.4.1. Stationary noise contributions

With reference to the stationary noise contributions, the ENC is given by [20,21]

$$\mathrm{ENC}^2 = \frac{A_1}{\tau_p}\frac{\alpha_A\eta_A\gamma_A 2kT}{g_{mA}}C^2 + A_2 A_{fA}\pi C^2 + A_3\tau_p\left[qI_{det} + 2kT\left(\frac{\alpha_A\eta_A g_{m1}^2}{g_{mA}} + \alpha_1\eta_1 g_{m1} + \frac{\alpha_2\eta_2 g_{m2}}{N^2} + \frac{1}{R_{F2}N^2}\right)\right] + A_4\pi\tau_p^2\left[g_{m1}^2(A_{fA} + A_{f1}) + \frac{g_{m2}^2 A_{f2}}{N^2}\right], \quad (7)$$

where $C = C_{in} + C_F$, A_1 to A_4 are coefficients which depend on the kind of shaping and τ_p is the shaped output pulse peaking time. By writing Eq. (7) we assumed that $R_{F2} = \mathrm{Re}\{1/Z_{F2}\}$ is independent of the frequency, as it verifies when Z_{F2} sets the first pole of the shaper. By considering that M_1 and M_2 are characterized by $L_2 = L_1$, $W_2 = N \times W_1$ and $V_{GS1} = V_{GS2}$, it follows that $A_{f2} = A_{f1}/N$, $g_{m2} = N \times g_{m1}$. For $N \gg 1$, Eq. (6) reduces to

$$\mathrm{ENC}^2 = \frac{A_1}{\tau_p}\frac{\alpha_A\eta_A\gamma_A 2kT}{g_{mA}}C^2 + A_2\pi A_{fA}C^2 + A_3\tau_p\left[qI_{det} + 2kT\left(\frac{\alpha_A\eta_A g_{m1}^2}{g_{mA}} + \alpha_1\eta_1 g_{m1} + \frac{1}{R_{F2}N^2}\right)\right] + A_4\pi\tau_p^2[g_{m1}^2(A_{f1} + A_{fA})]. \quad (8)$$

It is worth noting that the coefficient A_4 of the last term of Eq. (8) is divergent for unipolar shapings [22]. Nevertheless, if we assume that an ac-coupling with relatively long time constant is present at the end of the detection channel (i.e. to simulate the switch on/off of the system), the convergence is achieved and the ENC can be evaluated.

With regard to the noise contribution of M_1, the value of K_{f1}, α_1, δ_1 and g_{m1} must be known. In order to evaluate g_{m1} and the coefficient α_1, a HSPICE BSIM level 13 simulation of the transconductance g_{m1} versus the drain current I_D can be plotted, as shown in Fig. 8.

Three regions of operation can be located, by considering that in weak inversion the diode-like

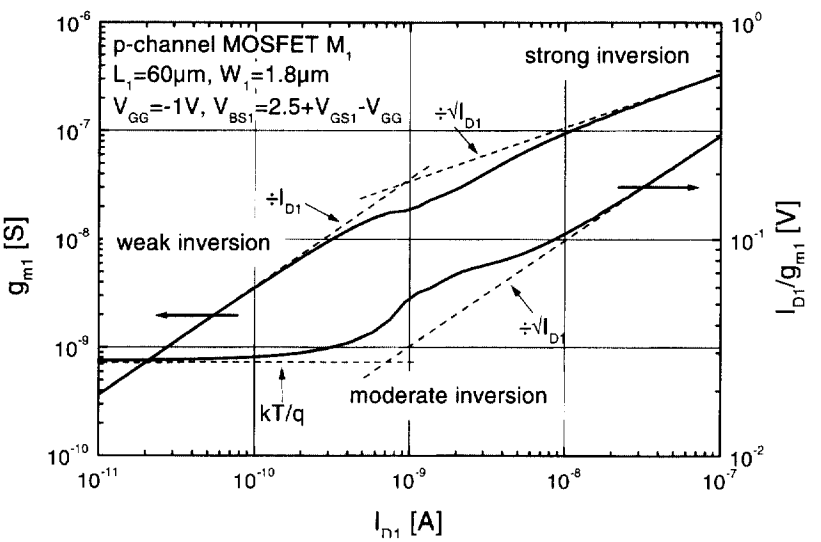

Fig. 8. Simulated g_{m1} and corresponding ratio I_{D1}/g_{m1} versus the drain current I_{D1}.

behavior of M_1 leads to $g_{m1} \div I_{D1}$ while in strong inversion it is $g_{m1} \div \sqrt{I_{D1}}$. In Fig. 8 is also plotted the ratio I_{D1}/g_{m1}, which approaches kT/q at the lowest I_{D1}. The value of α_1 can be deduced on the basis of Fig. 8 and the theoretical dependence of α_1 on I_{D1} [16]. With regards to the coefficient η_1, which depends on the bulk to source voltage V_{BS1} and it decreases as V_{BS1} increases, the evaluation is more difficult but a worst-case value $\eta_1 \approx 1.2$ can be assumed in most cases [15,16,23,24]. Finally, for the coefficient K_{f1}, which is stictly related to the technology, a value of 0.7×10^{-24} J is assumed.

In Fig. 9 is shown the ENC versus the output peaking time τ_p for a fifth-order complex unipolar Gaussian shaping [25], which offers good noise performance and is implemented by most of discrete commercial shaper amplifiers. In order to achieve the convergence of the fourth term of Eq. (8), an ac-coupling time constant of 1 s has been chosen. The corresponding values of the shaping coefficients are: $A_1 = 2.225$, $A_2 = 1.048$, $A_3 = 0.776$ and $A_4 = 5.329$ (A_4 rises to 7.888 for an ac-coupling time constant of 100 s). The ENC is evaluated for $C_{DET} = 1$ pF, $I_{DET} = 1$ nA and $N = 100$. For peaking times above few hundreds of nanoseconds, the main noise contributions are due to the shot noise of the detector leakage current and to the white noise associated with the reset device M_1. It is

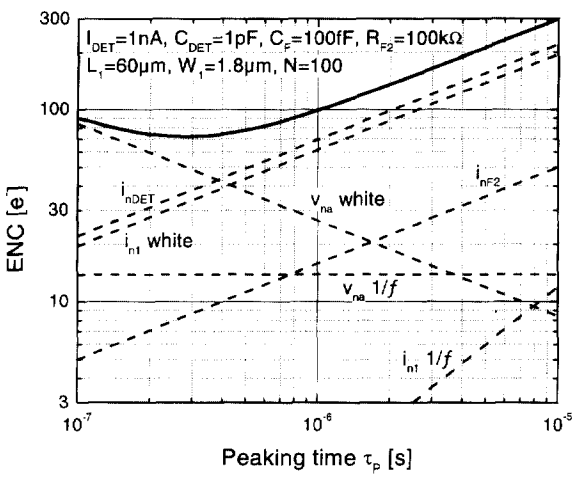

Fig. 9. ENC evaluated according to Eq. (8) for $I_{DET} = 1$ nA and $N = 100$.

worth noting that the white noise contribution of M_1 is lower than the noise contribution of I_{DET} and it corresponds, in this case, to an equivalent noise resistance close to 90 MΩ while the $1/f$ noise contribution of M_1 is negligible. The minor noise contribution due to R_{F2} can be further reduced by increasing N.

2.4.2. Non-stationary noise contributions

The non-stationary noise contributions related to the reset current can by evaluated by using the time-variant approach [26]. From Eq. (4) we can approximate the time dependence of the increment δg_{m1} of g_{m1}, which corresponds to each charge pulse Q_{DET} released by the detector, as

$$\delta g_{m1}(t) = k' \frac{W_1}{L_1} \frac{2(V_{GS1} - V_{T1})}{\left[2(V_{GS1} - V_{T1})\dfrac{C_F}{Q_{DET}} - 1\right] \exp\left(\dfrac{t}{C_F} g_{m1}\right) + 1} \times 1(t), \quad (9)$$

where g_{m1} is the transconductance of M_1 at the operating point and $1(t)$ is the step function. On the basis of the results of previous section, we can neglect all the non-stationary contributions related to an increment δg_{m1} of g_{m1}, except the one directly connected to the white term of i_{n1}. By using the generalized Campbell's theorem, we can represent this noise contribution with a sequence of unit-area δ-pulses with the time-dependent rate $2\,kT\alpha_1\eta_1\delta g_{m1}(t)$ [26–28]. The corresponding increase δENC_{M1} turns out to be

$$\delta ENC_{M1}^2 = \alpha_1\eta_1 2\,kT \int \delta g_{m1}(t) w(t)^2\, dt, \quad (10)$$

where $w(t)$ is the weighting function of the used shaper and we assumed, as a first approximation, that α_1 and η_1 do not change appreciably during the reset. The non-stationary noise contribution in Eq. (10) must be added to the corresponding stationary contribution $ENC_{M1}^2 = A_3\tau_p\alpha_1\eta_1 2kTg_{m1}$ of Eq. (8). In Fig. 10a are shown the sum $\sqrt{(ENC_{M1}^2 + \delta ENC_{M1}^2)}$ and the two single contributions as functions of the ratio Q_{DET}/C_F (i.e. the output peak voltage of the charge amplifier) for

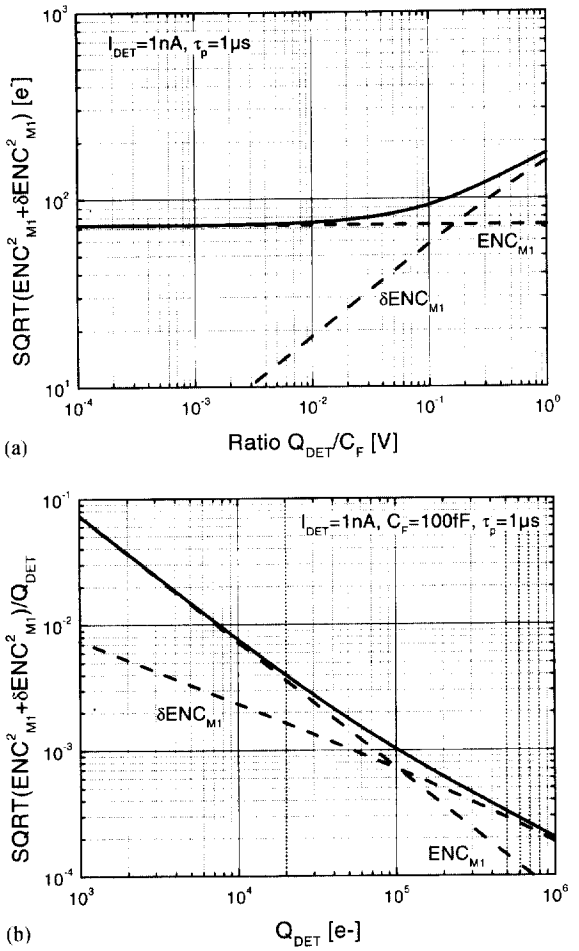

Fig. 10. (a) Sum $\sqrt{(\mathrm{ENC}_{\mathrm{M1}}^2 + \delta\mathrm{ENC}_{\mathrm{M1}}^2)}$ versus $Q_{\mathrm{DET}}/C_{\mathrm{F}}$; (b) noise/signal ratio $\sqrt{(\mathrm{ENC}_{\mathrm{M1}}^2 + \delta\mathrm{ENC}_{\mathrm{M1}}^2)}/Q_{\mathrm{DET}}$ versus Q_{DET}.

$I_{\mathrm{DET}} = 1$ nA and $\tau_{\mathrm{p}} = 1$ μs and for a fifth-order complex unipolar gaussian shaping. The increase in ENC due to the non-stationary noise contribution $\delta\mathrm{ENC}_{\mathrm{M1}}$ is non-negligible for values of $Q_{\mathrm{DET}}/C_{\mathrm{F}}$ above few mV. It can also be observed that $\delta\mathrm{ENC}_{\mathrm{M1}}$ is $\sim \div \sqrt{Q_{\mathrm{DET}}}$.

From an operative point of view it can be of higher interest to evaluate the noise to signal ratio $\sqrt{(\mathrm{ENC}_{\mathrm{M1}}^2 + \delta\mathrm{ENC}_{\mathrm{M1}}^2)}/Q_{\mathrm{DET}}$. This ratio is shown in Fig. 10b for $C_{\mathrm{F}} = 100$ fF. It can be observed that the noise/signal ratio is well below 1% for $Q_{\mathrm{DET}} > 10^4$ electrons and its increase, due to the non-stationary contribution, is relatively modest.

2.4.3. Total ENC

With regard to the total ENC, from Eqs. (8) and (10) we can write

$$\begin{aligned}\mathrm{ENC}^2 = {} & \frac{A_1}{\tau_{\mathrm{p}}}\frac{\alpha_{\mathrm{A}}\eta_{\mathrm{A}}\gamma_{\mathrm{A}}2kT}{g_{\mathrm{mA}}}C^2 + A_2\pi A_{\mathrm{fA}}C^2 \\ & + A_3\tau_{\mathrm{p}}\left\{qI_{\mathrm{det}} + 2kT\left[\frac{\alpha_{\mathrm{A}}\eta_{\mathrm{A}}g_{\mathrm{m1}}^2}{g_{\mathrm{mA}}}\right.\right. \\ & + \alpha_1\eta_1\left(g_{\mathrm{m1}} + \frac{1}{A_3\tau_{\mathrm{p}}}\int\delta g_{\mathrm{m1}}(t)w(t)^2\mathrm{d}t\right) \\ & \left.\left. + \frac{1}{R_{\mathrm{F2}}N^2}\right]\right\} + A_4\pi\tau_{\mathrm{p}}^2[g_{\mathrm{m1}}^2(A_{\mathrm{f1}} + A_{\mathrm{fA}})].\end{aligned} \tag{11}$$

In Fig. 11 is shown the ENC evaluated through Eq. (11) for different values of Q_{DET}. The corresponding non-stationary noise contribution $\delta\mathrm{ENC}_{\mathrm{M1}}$ for each case is also shown. It can be seen that the non-stationary contribution increases the ENC up to a factor 2 when the charge released by the detector increases of two orders of magnitude, from 1 fC up to 100 fC ($6.25 \times 10^5 \mathrm{e}^-$). Nevertheless, these noise performances can be considered acceptable in γ-ray and high-energy X-ray spectroscopy [29–35], where the resolution of the detector himself is limited to a FWHM $\approx 1\%$ at 660 keV (i.e. $\approx 600\mathrm{e}^-$ at $1.4 \times 10^5 \mathrm{e}^-$) at peaking times close to 1 μs.

From Fig. 11 it can also be observed that the slope of the non-stationary noise contribution $\delta\mathrm{ENC}_{\mathrm{M1}}$ decreases as the peaking time increases. This behavior can be explained by considering that for $\tau_{\mathrm{p}} \ll g_{\mathrm{m1}}/C_{\mathrm{F}}$ the $\delta g_{\mathrm{m1}}(t)$ factor of Eq. (10) is a slow function of time compared to the weighting function $w(t)$ and the $\delta\mathrm{ENC}_{\mathrm{M1}}$ behaves like a white parallel noise contribution. On the contrary, for $\tau_{\mathrm{p}} \gg g_{\mathrm{m1}}/C_{\mathrm{F}}$ the $\delta g_{\mathrm{m1}}(t)$ is a fast function of the time when compared to $w(t)$ and the $\delta\mathrm{ENC}_{\mathrm{M1}}$ is less dependent on τ_{p}. This effect is more evident at the highest values of Q_{DET}, where the reset signal is faster.

2.4.4. Choice of the bias point of M_1

From the results of previous analysis, some design criteria for the choice of the bias point and

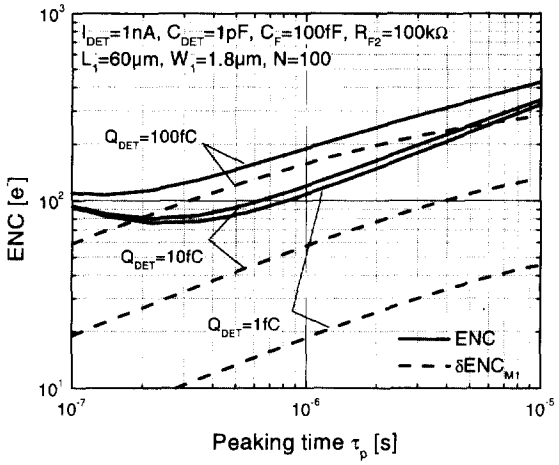

Fig. 11. ENC versus the peaking time τ_p evaluated for different values of Q_{DET}. For each case, the non-stationary noise contribution δENC_{M1} (dashed line) is also shown.

geometry of M_1, once the detector current I_{DET} (i.e. the drain current I_{D1}) is given, can be drawn out. Only the white noise contribution of M_1 will be considered, assuming the $1/f$ term negligible.

A first design criterion regards the choice of the drain to source voltage V_{DS1} of M_1. Once the gate geometry (see second design criterion) and the drain current I_{D1} are fixed, the value of V_{GG} can be chosen in order to let M_1 operate in the linear region ($|V_{DS1}| < |V_{GS1} - V_{T1}|$) or in the saturation region ($|V_{DS1}| > |V_{GS1} - V_{T1}|$). Starting from the bias point $|V_{DS1}| = |V_{GS1} - V_{T1}|$, an increase of V_{GG} leads to an increase of $|V_{DS1}|$ while $|V_{GS1} - V_{T1}|$ and g_{m1} do not change appreciably, so that no change in the noise performances of M_1 can be expected. On the contrary, if V_{GG} decreases, M_1 enters the linear region. Neglecting for simplicity the effect of the fixed bulk charges and assuming $\alpha_1 \approx 1$ for the noise coefficient in the saturation region, we can approximate the ratio between the white noise of M_1 in the linear region and in the saturation region as follows [6]:

$$\frac{2kTk'\frac{W_1}{L_1}|V_{GS1Lin} - V_{T1}|}{2kTk'\frac{W_1}{L_1}|V_{GS1} - V_{T1}|} = \frac{|V_{GS1lin} - V_{T1}|}{|V_{GS1} - V_{T1}|}, \quad (12)$$

where V_{GS1LIN} is the drain to source voltage in the linear region. Equating the expressions for the current in the linear and saturation region we can also write

$$\frac{1}{2}k'\frac{W_1}{L_1}[2|V_{GS1Lin} - V_{T1}|V_{DS1} - V_{DS1}^2] = \frac{1}{2}k'\frac{W_1}{L_1}|V_{GS1} - V_{T1}|^2, \quad (13)$$

and, solving for $|V_{GS1LIN}\text{-}V_{T1}|$, it follows:

$$|V_{GS1Lin} - V_{T1}| = \frac{V_{DS1}}{2}\left[1 + \left(\frac{|V_{GS1} - V_{T1}|}{V_{DS1}}\right)^2\right] > |V_{GS1} - V_{T1}|, \quad (14)$$

where the condition $|V_{DS1}| < |V_{GS1} - V_{T1}|$ must be satisfied. From Eqs. (12) and (14) it turns out that a higher white noise contribution from M_1 can be expected when it is biased in the linear region. The first design criterion for the choice of the bias point is that M_1 must operate in the saturation region.

A second design criterion regards the choice of the gate geometry (L_1, W_1) of M_1. Once the drain current I_{D1} is fixed and assuming that M_1 is in the saturation region, the value of the ratio W_1/L_1 can be chosen in order to let M_1 operate in weak inversion ($|V_{GS1}| < |V_{T1}|$) or in strong inversion ($|V_{GS1}| > |V_{T1}|$). From Fig. 8 it can be seen that the ratio I_{D1}/g_{m1} is higher in the latter region of operation. Neglecting for simplicity the effect of the fixed bulk charges and assuming $\alpha_1 \approx 1$, it follows that the white noise contribution of M_1, which is proportional to g_{m1}, is lower in the strong inversion region of operation at equal I_{D1}. Moreover, by considering that in the strong inversion $g_{m1} \doteq \sqrt{(I_{D1}W_1/L_1)}$ it follows that a L_1/W_1 ratio as high as possible must be chosen, which means also a $|V_{GS1} - V_{T1}|$ as high as possible. The second design criterion for the choice of the bias point and the gate geometry is that M_1 must operate, if possible, in the strong inversion, and in any case with a maximized L_1/W_1 ratio.

It is worth noting that the optimization must be carried out with reference to the minimum value I_{DETmin} of the expected detector leakage current I_{DET}. In fact, it can be easily deduced from previous

analysis that, once the gate geometry and bias point of M_1 are optimized for $I_{D1} = I_{DETmin}$, the ratio between the shot noise of I_{DET} and the noise contribution of M_1 increases with I_{DET}. Thus, the target of the minimization of the noise contribution of the reset system with respect to the noise contribution of the detector leakage current is achieved for all values of $I_{DET} \geq I_{DETmin}$.

2.4.5. Noise of the reset system at high rates

If the average rate $1/T_R$ of the charge pulses from the detector is small compared to the time required by the reset system to remove the charge of each ionizing event, no pile-up of the reset current pulses occurs. As the average rate $1/T_R$ increases, not all the charge released at a given ionizing event is removed from the input node before the arrival of the next charge pulse, and the pile-up of the reset current pulses occurs. Due to the pile-up, the average reset current increases and consequently the noise associated to the reset current increases.

The total increase $\delta_R ENC_{M1}$ can be evaluated again through Eq. (10) replacing $\delta g_{m1}(t)$, associated to the single reset current pulse, with $\delta_R g_{m1}(t)$, associated to the total reset current (sum of the single reset current pulses):

$$\delta_R ENC_{M1}^2 = \alpha_1 \eta_1 2kT \int \delta_R g_{m1}(t) w(t)^2 \, dt. \tag{15}$$

In Fig. 12 are shown the total increment $\delta_R g_{m1}(t)$, the single contributions $\delta g_{m1}(t + T_n)$ (assuming the same Q_{DET} for each event) and the weighting function $w(t)^2$ evaluated using the same parameters of previous examples. The parameter T_n is the time interval between the nth reset pulse (going backward in time) and the last reset pulse ($n = 0$), which is related to the event of interest ($t = 0$).

For simplicity, in this analysis we will neglect the change in the time constant C_F/g_{m1} of Eq. (9) which is due to the shift of the baseline, and we will solve Eq. (15) for low enough values of Q_{DET} such that $2(V_{GS1} - V_{T1})C_F/Q_{DET} \gg 1$. This approximation leads to a worst case evaluation of Eq. (15), because for higher values of Q_{DET} or g_{m1} the pile-up effect is expected to be smaller, due to the smaller duration of the reset pulses (see Fig. 4b). The total increment $\delta_R g_{m1}(t)$ can be written:

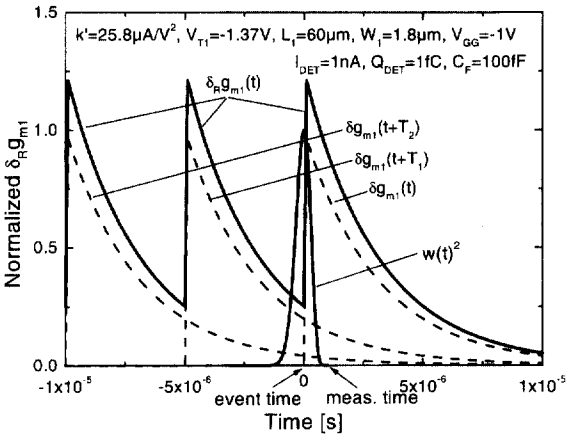

Fig. 12. Total increment $\delta_R g_{m1}(t)$, single contributions $\delta g_{m1}(t + T_n)$ (assuming the same Q_{DET} for each event) and weighting function $w(t)^2$ for a fifth-order complex unipolar Gaussian shaping versus the time.

$$\delta_R g_{m1}(t) \approx \sum_{n=0}^{+\infty} \delta g_{m1}(t + T_n) \approx \sum_{n=0}^{+\infty} k' \frac{W_1}{L_1} \frac{Q_{DETn}}{C_F} \times \exp\left(-\frac{t + T_n}{C_F} g_{m1}\right) 1(t + T_n), \tag{16}$$

where Q_{DETn} is the charge released at the nth event. By substituting Eq. (16) into Eq. (15) we get

$$\begin{aligned}
\delta_R ENC_{M1}^2 &= \alpha_1 \eta_1 2kT \int \delta_R g_{m1}(t) w(t)^2 dt \\
&\approx \alpha_1 \eta_1 2kT \int \sum_{n=0}^{\infty} k' \frac{W_1}{L_1} \frac{Q_{DETn}}{C_F} \times \exp\left(-\frac{t + T_n}{C_F} g_{m1}\right) 1(t + T_n) w(t)^2 \, dt \\
&\approx \alpha_1 \eta_1 2kT \int \sum_{n=0}^{\infty} k' \frac{W_1}{L_1} \frac{1}{C_F} \exp\left(-\frac{t}{C_F} g_{m1}\right) 1(t) \times \left[Q_{DET} + 2 \sum_{n=1}^{\infty} Q_{DETn} \exp\left(-\frac{T_n}{C_F} g_{m1}\right) \right] w(t)^2 \, dt \\
&\approx \left[1 + 2 \frac{\overline{Q_{DET}}}{Q_{DETn}} \sum_{n=1}^{\infty} \exp\left(-\frac{T_n}{C_F} g_{m1}\right) \right] \delta ENC_{M1}^2,
\end{aligned} \tag{17}$$

where $\delta\mathrm{ENC}_{\mathrm{M1}}$ is the increase at low rates (calculated in Section 2.4.2), $\overline{Q_{\mathrm{DET}}}$ is a weighted average of all amplitudes of the spectrum under consideration and we approximated, for $n > 0$, $1(t + T_n) \approx 2 \times 1(t)$ by considering that $\delta g_{\mathrm{m1}}(t + T_n)$ is a slow function of the time with respect to $w(t)$, which is assumed to be symmetrical (see Fig. 12). The sum of Eq. (17) gives the increase in ENC due to the rate and can be evaluated once the distribution of the times of arrival of the charge pulses from the detector is known. In the case of a Poisson distribution of the time intervals between the charge pulses, the Erlang distribution [27] of the T_n must be used. Running the average:

$$\int_0^{+\infty} \sum_{n=0}^{\infty} \frac{1}{n!}\left(\frac{T}{T_{\mathrm{R}}}\right)^n \mathrm{e}^{-Tg_{\mathrm{m1}}/C_{\mathrm{F}}}\, \mathrm{e}^{-T/T_{\mathrm{R}}} \mathrm{d}\left(\frac{T}{T_{\mathrm{R}}}\right)$$

$$= \int_0^{+\infty} \mathrm{e}^{-Tg_{\mathrm{m1}}/C_{\mathrm{F}}}\, \mathrm{e}^{-T/T_{\mathrm{R}}} \sum_{n=0}^{\infty} \frac{1}{n!}\left(\frac{T}{T_{\mathrm{R}}}\right)^n \mathrm{d}\left(\frac{T}{T_{\mathrm{R}}}\right)$$

$$= \int_0^{+\infty} \mathrm{e}^{-Tg_{\mathrm{m1}}/C_{\mathrm{F}}}\, \mathrm{d}\left(\frac{T}{T_{\mathrm{R}}}\right) = \frac{C_{\mathrm{F}}}{g_{\mathrm{m1}} T_{\mathrm{r}}}, \tag{18}$$

where $1/T_{\mathrm{R}}$ is the average rate. Replacing in Eq. (17), we obtain

$$\delta_{\mathrm{R}}\mathrm{ENC}_{\mathrm{M1}}^2 = \left[1 + 2\frac{\overline{Q_{\mathrm{DET}}}}{Q_{\mathrm{DET}}}\frac{C_{\mathrm{F}}}{g_{\mathrm{m1}} T_{\mathrm{R}}}\right]\delta\mathrm{ENC}_{\mathrm{M1}}^2, \tag{19}$$

which shows that the increase in ENC due to the rate is proportional to the square root of the ratio between the decay time constant $C_{\mathrm{F}}/g_{\mathrm{m1}}$ and the average time interval T_{R}.

2.5. Layout considerations

On the basis of the results of previous sections, we can conclude that: (i) in order to minimize the stationary noise contribution of M_1, high values of the L_1/W_1 ratio should be used; (ii) in order to minimize the stationary noise contributions of next stages (M_2, R_{F2}), high values of the ratio N should be used and (iii) in order to minimize the non-stationary noise contribution of M_1, high values of the L_1/W_1 ratio and high values of C_{F} (at equal Q_{DET}) should be used. The drawback of all these solutions lies in the increase of the layout area which realizes the reset with respect to the area of the whole channel. In Fig. 13a and b are shown respectively the layout of the circuit of Fig. 5 and the layout of the complete detection channel (which implements also the fifth-order complex unipolar Gaussian shaping), for a 1.2 μm CMOS technology. We assumed $L_1 = 60$ μm, $W_1 = 1.8$ μm, $C_{\mathrm{F}} = 100$ fF and $N = 150$. In order to achieve a reliable N factor, we designed M_2 and C_{O} as N copies of M_1 and C_{F}, respectively.

In this case it can be seen that the area occupied by the reset circuit (i.e. the area occupied by M_2 and $C_{\mathrm{O}} \approx 150$ μm × 780 μm) is close to the 51% of the circuit of Fig. 5 (≈ 220 μm × 1020 μm). On the

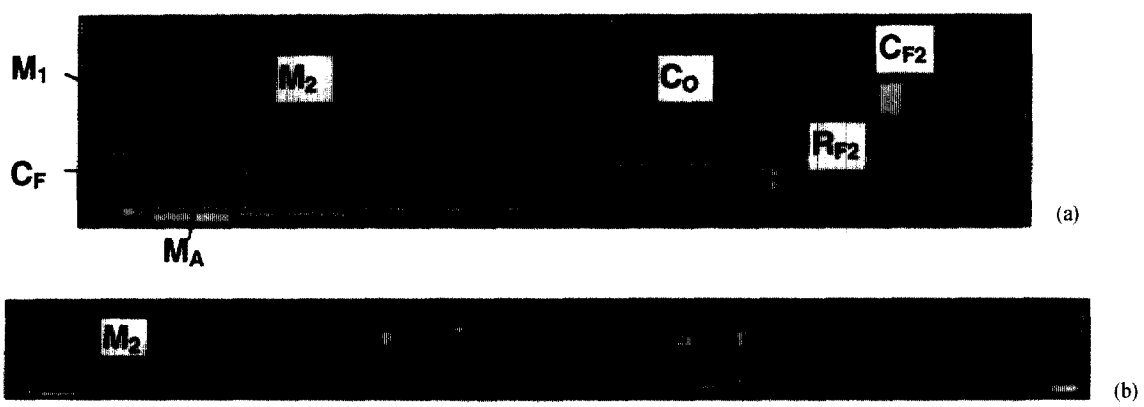

Fig. 13. Layout: (a) of the circuit of Fig. 5; (b) of the complete detection channel.

other hand, when compared to the area of the complete detection channel it reduces to the 21% of the overall circuit.

3. Conclusions

A theoretical analysis of a compensated continuous reset system, based on the use of p-channel MOSFETs operating in the saturation region, has been presented. The system is self-adaptable with respect to a wide range of detector leakage currents. The HSPICE BSIM level 13 simulations of the static and dynamic performances, as well as the evaluation of the signal/noise performances, which take into account the stationary and non-stationary noise contributions at low and high rates, show that the system can be useful in γ-ray and high-energy X-ray spectroscopy. The analysis, focused on detectors characterized by a 1 nA leakage current, can be easily extended to other cases and applications. In order to verify the presented results, an experimental investigation will be carried out in near future.

Acknowledgements

The authors wish to thank Pavel Rehak for the useful suggestions and comments. The work is supported by the eV Products, Division of II-VI Inc., USA and by the US Department of Energy, Contract No. DE-AC02-98CH10886.

References

[1] D.A. Landis, C.P. Cork, N.W. Madden, F.S. Goulding, IEEE Trans. Nucl. Sci. NS-29 (1) (1982) 619.
[2] C.L. Britton, T.H. Becker, T.J. Paulus, R.C. Trammell, IEEE Trans. Nucl. Sci. NS-31 (1) (1982) 455.
[3] W. Buttler, B.J. Hosticka, G. Lutz, Nucl. Instr. and Meth. A 288 (1990) 187.
[4] E. Beuville, K. Borer, E. Chesi, E.H.M. Heijne, P. Jarron, B. Lisowski, S. Singh, Nucl. Instr. and Meth. A 288 (1990) 157.
[5] F. Krummenacher, Nucl. Instr. and Meth. A 305 (1991) 527.
[6] P. O'Connor, G. Gramegna, P. Rehak, F. Corsi, C. Marzocca, IEEE Trans. Nucl. Sci. 44 (1997) 318.
[7] P. O'Connor, G. Gramegna, P. Rehak, S. Hart, Nucl. Instr. and Meth. A 390 (1997) 241.
[8] W.W. Moses, I. Kipnis, M.H. Ho, IEEE Trans. Nucl. Sci. NS-41 (4) (1994) 1469.
[9] B. Ludewigt, J. Jaklevic, I. Kipnis, C. Rossington, H. Spieler, IEEE Trans. Nucl. Sci. NS-41 (4) (1994) 1037.
[10] R.L. Chase, A. Hrisoho, J.P. Richer, 7th Pisa Meet. on Adv. Detectors, La Biodola, Isola d'Elba, Italy, May 1997.
[11] E. Beuville, P. Barale, F. Bieser, W. Hearn, S.R. Klein, M.A. Lisa, T. Noggle, H.G. Ritter, C. Vu, H. Wienman, Internal Report, Lawrence Berkeley National Laboratory.
[12] J.C. Santiard, W. Beush, S. Buytaert, C.C. Enz, E. Heijne, P. Jarron, F. Krummenacher, K. Marent, F. Piuz, 6th Pisa Meet. on Adv. Detectors, La Biodola, Isola d'Elba, Italy, May 1994.
[13] H.T.H. Piaggio, Differential Equations, G. Bell&Sons, London, 1965.
[14] J. Chang, A.A. Abidi, C.R. Viswanathan, IEEE Trans. Electron. Dev. 41 (11) (1994) 1965.
[15] S. Tedja, H.H. Williams, J. Van der Spiegel, F.M. Newcomer, R. Van Berg, IEEE Trans. Electron. Dev. 41 (11) (1994) 2069.
[16] S. Tedja, J. Van der Spiegel, H.H. Williams, IEEE Trans. Electron. Dev. 41 (11) (1994) 2069.
[17] A. Abidi, IEEE Trans. Electron. Dev. 33 (11) (1986) 1801.
[18] R.P. Jindal, IEEE Trans. Electron. Dev. 33 (9) (1986) 1395.
[19] R. Sarpeshkar, T. Delbrück, C.A. Mead, IEEE Circuits & Devices 1993.
[20] E. Gatti, M. Sampietro, P.F. Manfredi, Nucl. Instr. and Meth. A 287 (1990) 513.
[21] G. De Geronimo, 5th Int. Workshop on GaAs & Rel. Comp., Cividale, Italy, June 1997, Nucl. Instr. and Meth. A 410 (1998) 124.
[22] G.E. Gatti, Nucl. Instr. and Meth. A 361 (1995) 277.
[23] B. Wang, J.R. Hellums, C.G. Sodini, IEEE J. Solid-State Circuits, 29 (7) (1994) 833.
[24] T. Sah, S.Y. Wu, F.H. Hielscher, IEEE Trans. Electron. Dev. 13 (4) (1966) 410.
[25] S. Ohkawa, M. Yoshizawa, K. Husimi, Nucl. Instr. and Meth. 138 (1976) 85.
[26] E. Gatti, P.F. Manfredi, La Rivista del Nuovo Cimento, 9 (1986) 1.
[27] A. Papoulis, Probability, Random Variables, and Stochastic Processes, McGraw-Hill, New York, 1991.
[28] T.H. Wilmshurst, Signal Recovery, Adam Hilger, Bristol, 1990.
[29] Z. He, G.F. Knoll, D.K. Wehe, J. Miyamoto, IEEE Nucl. Sci. Symp., Anaheim, USA, November 1996.
[30] J.C. Lund, J.M. VanScyoc III, R.B. James, D.S. McGregor, R.W. Olsen, Nucl. Instr. and Meth. A 380 (1996) 256.
[31] M.R. Squillante, G. Entine, Nucl. Instr. and Meth. A 380 (1996) 160.
[32] R. Arlt, D.E. Rundquist, Nucl. Instr. and Meth. A 380 (1996) 455.
[33] C. Scheiber, Nucl. Instr. and Meth. A 380 (1996) 385.
[34] P.N. Luke, Nucl. Instr. and Meth. A 380 (1996) 232.
[35] eV Products, personal communication, 1998.